ence that this feature may represent an evolving intrusive boundary at the top of a partial-melt zone.

REFERENCES AND NOTES

1. K. D. Nelson *et al.*, *Science* **274**, 1684 (1996).
2. Before processing the data the ground displacement was restored at all broadband and short period stations. Each seismogram was rotated from the standard vertical, north and east coordinate system into a ray system [Longitudinal (*L*) and *T* components] using the eigenvalues of the covariance matrix for the computation of the rotation angles at a time window following the *P*-wave arrival. The *L* and *Q* components result from a rotation of *Z* (vertical) and *R* (radial) around the angle of incidence of the *P* wave. The *Q* component is perpendicular to the incoming *P* phase in the plane of incidence and contains mostly *SV* energy and little *P*-wave energy. Source equalization was accomplished by deconvolution of the *Q* component with the *P* wave of the *L* component.
3. R. Kind, G. L. Kosarev, N. V. Peterson, *Geophys. J. Int.* **121**, 191 (1995).
4. N. A. Haskell, *J. Geophys. Res.* **67**, 4751 (1990).
5. Trace A36 results from averaging receiver functions from BB10, BB36, and SP12 and trace A18 is an averaging of receiver functions from stations BB34, BB18, and BB20.
6. L. D. Brown *et al.*, *Science* **274**, 1688 (1996).
7. The two-station phase velocity dispersion of the fundamental mode Rayleigh wave was computed using programs developed by R. Herrmann. In the data analysis we first extracted the group velocity dispersion curve of the fundamental mode by applying a Gabor Transform to the recorded Rayleigh wave train. The fundamental mode Rayleigh waveforms were isolated from the recorded Rayleigh waves by applying a phase match filter.
8. J. Wu *et al.*, *Eos* **76**, F392 (1995).
9. L.-S. Zhao and C. Frohlich, *Geophy. J. Int.* **124**, 525 (1996); L.-S. Zhao, M. K. Sen, P. Stoffa, C. Frohlich, *ibid.* **125**, 355 (1996).

10. We thank I. Billings, M. Brunner, A. Fabritius, S. Klemperer, Y. Makovksy, K. Wu, and Chinese scientists in helping to collect the seismic data used in this study. This research was funded by the National Science Foundation Grant NSF EAR-9316814.

2 August 1996; accepted 5 November 1996

Electrically Conductive Crust in Southern Tibet from INDEPTH Magnetotelluric Surveying

Leshou Chen, John R. Booker, Alan G. Jones,* Nong Wu, Martyn J. Unsworth, Wenbo Wei, Handong Tan

The crust north of the Himalaya is generally electrically conductive below depths of 10 to 20 km. This conductive zone approaches the surface beneath the Kangmar dome (dipping north) and extends beneath the Zangbo suture. A profile crossing the northern Yadong-Gulu rift shows that the high conductivity region extends outside the rift, and its top within the rift coincides with a bright spot horizon imaged on the INDEPTH CMP (common midpoint) profiles. The high conductivity of the middle crust is atypical of stable continental regions and suggests that there is a regionally interconnected fluid phase in the crust of the region.

The INDEPTH magnetotelluric (MT) investigation undertaken during April to July of 1995 was designed to study the electrical structure of the lithosphere beneath southern Tibet. Two earlier MT studies were carried out in the region: A Sino-French group collected MT data in southern Tibet in the early 1980s (*1*), and, subsequently, MT data were collected by Chinese investigators as part of the Golmud to Yadong Global Geoscience Transect activities (*2*). The INDEPTH MT study provided closely spaced sites and a wide frequency bandwidth compared to these surveys, and substantiated several of their conclusions.

We acquired MT data along two lines—a main north-south line that extended from the crest of the Himalaya to near Yangbajain in the Lhasa block [100-line, figure 1 of (*3*)], and a northwest-southeast trending line that obliquely crossed the northern Yadong-Gulu rift near Damxung (200-line) (*4*). The MT data were recorded with the use of two systems: a five-component commercial wideband system (Phoenix V5) for shallow probing, and 20 five-component recording systems (GSC LIMS) for deeper penetration (*5*, *6*). During the period of LIMS acquisition, 24 March to 31 July 1995, sunspot activity was low, resulting in poor signal. We compensated for this by recording for a longer interval at each location than originally planned (4 to 5 weeks instead of 2 to 3 weeks), resulting in fewer total sites than planned for the experiment.

Distortion analysis (*7*) was applied to the MT response estimates, both in single-frequency, single-site and in multi-frequency, multi-site modes, to determine the dimensionality of the data and derive the dominant electric strike direction. The distortion models fit the data well, which implies that a two-dimensional (2D) description of regional structures is a reasonable assumption. The electric strike directions at frequencies sampling the thick Tibetan crust beneath the 100-line are frequency-independent and east-west for most sites—parallel to the regional surface geologic strike. This observation suggests that the surface geologic strike in the region is representative of structure throughout the thickness of the crust sensed by the MT survey, which is not always the case in orogenic belts (*8*).

For both lines, the phase difference between the electric and magnetic fields, in both polarizations of induction (*9*), was greater than 45° at all but a few sites and increased with increasing period. This result indicates that conductivity increases in the crust (resistivity decreases) with increasing depth (*10*). Apparent resistivities were low, $<10\ \Omega \cdot m$, at frequencies less than 0.1 Hz, and for some sites the apparent resistivities were below $1\ \Omega \cdot m$ for frequencies less than 0.01 Hz. Such pervasively low values are atypical in the continents; shield regions have apparent resistivities that are more than two orders of magnitude higher.

We modeled the MT data using 2D inversion algorithms that simultaneously searched for the smoothest as well as best-fitting models (*11*) (Figs. 1 and 2). The data can be fit by more complex models, but models with less structure result in unacceptable misfits.

The model for the 100-line is based on the MT and vertical-field transfer-function data at 13 frequencies, from 80 to 0.0015 Hz, from all sites, and fits the data with an average RMS misfit of 10° in phase, 5% in apparent resistivity, and 0.10 in GDS transfer function. These misfits are high, but most misfit is concentrated on data from the southernmost four sites, which were found impossible to model because their responses were inconsistent between the two modes.

The model exhibits the following first-order features that are apparent in the data, appeared in all inversions for different frequency and site subsets and different assumptions about static shifts (*12*), and were not influenced by the abherent responses just mentioned: (i) From approximately 150 km south of the Zanbo suture to the north end of the line, the crust is generally electrically conductive below depths of 10 to 20 km ($<200\ \Omega \cdot m$). (ii) North of Kangmar the crust becomes extremely conductive at depth (generally much less than $30\ \Omega \cdot m$; "3" in Fig. 1). (iii) A north-dipping zone of high conductivity extends upward to the

Leshou Chen, Wenbo Wei, Handong Tan, China University of Geosciences, Beijing, China.
J. R. Booker, Nong Wu, M. J. Unsworth, School of Geophysics, University of Washington, Seattle, WA 98195, USA.
A. G. Jones, Geological Survey of Canada, 1 Observatory Crescent, Ottawa, Ontario, Canada K1A 0Y3.
* To whom correspondence should be addressed.

near-surface beneath the Kangmar dome ("2" in Fig. 1). At depth this zone appears to connect with the midcrustal zone of high conductivity to the north. (iv) The uppermost crust beneath the Zangbo suture contains a narrow electrically conductive body ("1" in Fig. 1). The suture has no electrical expression below a depth of a few kilometers.

The model for the 200-line data crossing the northern Yadong-Gulu rift fits the long-period (frequencies <1 Hz) MT data with an average misfit of 2° in phase, and equivalent level in apparent resistivity. The model shows the following (Fig. 2): (i) Electrical conductivity is high below depths of 10 to 20 km across the entire profile (<200 m). (ii) The conductive middle crust contains several zones of high conductivity at depths below depths of 15 to 20 km (few $\Omega \cdot$ m; "1", "2", and "3" in Fig. 2). The top of the center one ("2" in Fig. 2) coincides within resolution with the YDR bright spot horizon imaged on the INDEPTH CMP profile [see figure 1 of (*13*)]. (iii) A shallow southeast-dipping zone of enhanced conductivity extends from the near surface near Nam Tso to a depth of about 10 km beneath the Damxung graben ("4" in Fig. 2).

The sharply decreasing electrical resistivity with depth over most of the survey, and in particular the midcrustal resistivities of about 1 to 10 $\Omega \cdot$ m north of Kangmar, substantiates the observation that this region has high crustal conductivity (*1,2*). The midcrustal conductivity is so high north of Kangmar that we are unable to characterize the conductivity of the lowermost crust or underlying mantle of the region. As dry rocks typically have resistivities in the hundreds to thousands of $\Omega \cdot$ m (*14*), the low midcrustal resistivity north of about Kangmar suggests that an interconnected fluid phase is present within the crust. Given that heat flow in this region is highest near the latitude where the conductive anomaly is closest to the surface (242 mW/m^2) (*15*), the presence of partial melt offers a ready explanation for the data that does not require unusual conditions for continental crust.

The observation that the Zangbo suture zone anomaly is limited to the upper few kilometers of the crust suggests the midcrustal partial melt zone is superposed across the suture at depth or that the suture is cut off by a fault in the upper crust. The anomalously conductive material extending upward toward the surface at the Kangmar dome suggests that partially molten material has been transported relatively upward beneath the north flank of the Kangmar anticlinorium. This might either be as an intrusion or transport in the hanging wall of a thrust. Alternatively, saline fluid trapped in porous subducted sediments is also a candidate for this anomaly (*16*).

The observation from the 200-line that conductive middle crust extends beyond the surface expression of the Yadong-Gulu rift (Damxung graben/Nyainqentanglha range) implies that the mid-crustal partial melt extends outside the immediate confines of the rift. Finally, the shallow high-conductivity feature imaged on the 200-line ("4" in Fig. 2) suggests that deep hydrothermal fluids are present deep beneath Nam Tso (perhaps circulating to depth along a normal fault).

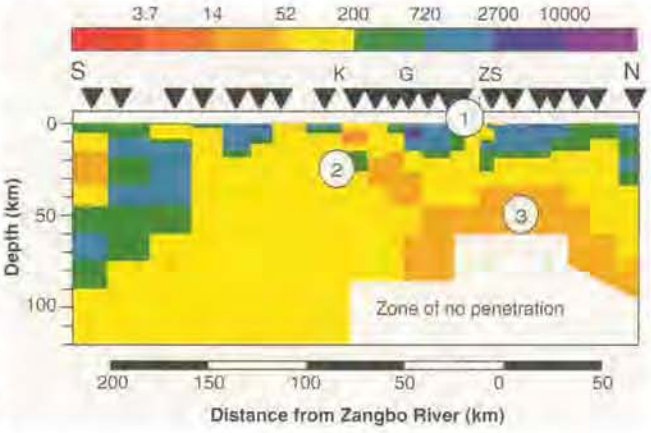

Fig. 1. Resistivity model for the north-south 100-line data from Yadong in the south (left-hand side) to almost Yangbajain in the north (right-hand side). Hotter colors (reds) indicate zones of enhanced electrical conductivity (resistivity <30 $\Omega \cdot$ m), whereas colder colors (greens and blues) indicate zones of low conductivity (resistivity >200 $\Omega \cdot$ m). Note that the high conductivity in the midcrust beneath the northern half of the line precluded penetration of EM fields into the mantle ("zone of no penetration"). ZS, Zangbo suture; G, Gyandse; K, Kangmar. The inverted triangles denoted the locations of the LIMS/V5 sites. Numbers refer to features discussed in the text.

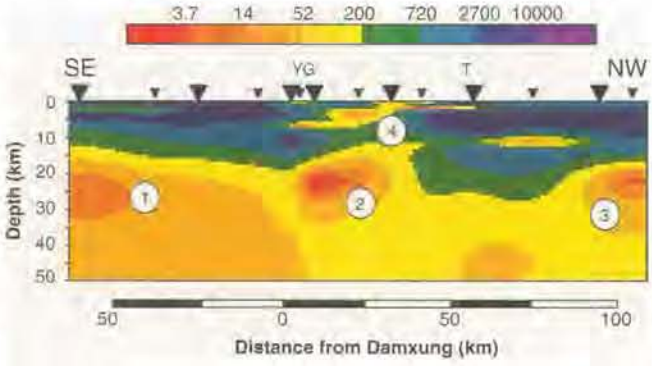

Fig. 2. Resistivity model for the north-south 200-line data from Nam Tso to the northwest (right hand side) to north of Dagze to the southeast (left hand side). Colors as in Fig. 1. YG, Yangbajain-Damxung graben; T, Thak. The large inverted triangles denote the locations of the LIMS/V5 sites, whereas the small inverted triangles denote the locations of the V5-only sites. Numbers refer to features discussed in the text.

REFERENCES AND NOTES

1. Pham Van Ngoc *et al.*, *Nature* **311**, 615 (1986).
2. Guo Xinfeng, Zhang Yuanchou, Cheng Qingyun, Gao Rui, Pan Yu, *Bull. Chin. Acad. Geol. Sci.* **21**, 191 (1990) (In Chinese with English abstract). See Wu Gong-jian *et al.*, *Chin. J. Geophys.* **35**, 195 (1992).
3. K. D. Nelson *et al.*, *Science* **274**, 1684 (1996).
4. The experiment was a tri-national effort between scientists at the University of Washington (UW), the Geological Survey of Canada (GSC), and the China University of Geosciences (CUG) in Beijing. The North American groups were responsible for acquisition of deep-probing MT data at 35 locations, while the Chinese group recorded shallower-probing data at the same locations and others in between.
5. The V5 system records data from 0.003 to 100 Hz and is typically sensitive to electrical conductivity from close to the surface (1 km) to the base of the continental crust (30 km), but here to about the middle of the overthickened Tibetan crust. The GSC-designed LIMS (long-period magnetotelluric system) acquires low-frequency data (0.0003 to 0.05 Hz, or a periodicity of 20 to 30,000 s), and samples usually from about a depth of 5 km to deep within the subcrustal lithosphere (>250 km), but here to only 100 km or less because of the high conductivities encountered at depth. The LIMS data for the 100-line used station 201 at Dagze as a remote-reference. For the 200-line data the LIMS data were referenced against each other. The V5 data were not remote-reference processed as only one system was available, but impedance bias effects were not significant. Recording durations at a site were usually 20 to 30 hours with the V5, and 3 to 7 weeks with each LIMS.
6. Initial processing was done in the field to ensure that significant conductivity features were not spatially undersampled. The time series data from both systems were processed and merged to yield MT response estimates at each site covering seven decades of frequency, and these estimates were analyzed for distortions, dimensionality, and strike direction.
7. R. W. Groom and R. C. Bailey, *J. Geophys. Res.* **94**, 1913 (1989). For applications of Groom-Bailey decomposition, see, for example, A. G. Jones and I. Dumas, *Phys. Earth Planet. Inter.* **81**, 289 (1993); R. W. Groom, R. D. Kurtz, A. G. Jones, D. E. Boerner, *Geophys. J. Int.* **115**, 1095 (1993); (*8*).
8. G. Marquis, A. G. Jones, R.D. Hyndman, *Geophys. J. Int.* **120**, 111 (1995).
9. For a two-dimensional (2D) Earth, the electromagnetic fields decouple into two modes. One mode is for current flowing along the structure and is called the transverse-electric, or TE, mode. The other mode is for current flowing across the structure and is the transverse-magnetic, or TM, mode.
10. Over a uniform half space, the MT phase is 45°. If conductivity increases with depth, then the phases

will be greater than 45°. Conversely, if conductivity decreases with depth, then the phases will be less than 45°. The phases are preferred as qualitative indicators, as they are unaffected by galvanic static shifts *(12)* that often distort apparent resistivity curves. At most sites, the apparent resistivity curves of the two modes (TE and TM) *(9)* coalesced at high frequencies (>30 Hz).

11. C. deGroot-Hedlin and S. C. Constable, *Geophysics* **55**, 1613 (1990). J. T. Smith and J. R. Booker, *J. Geophys. Res.* **96**, 3905 (1991).
12. Static shifts of MT data are so-called because local, small-scale scatterers will distort the amplitudes of the electric field but not affect the phase nor the magnetic field. This condition leads to a period-independent multiplicative shift of the apparent resistivity curve, causing model depths to be in error. See A.G. Jones, *Geophysics* **53**, 967 (1988). These data were surprisingly little affected by severe static shift problems.
13. L. D. Brown *et al.*, *Science* **274**, 1688 (1996).
14. A. G. Jones, in *Continental Lower Crust*, D. M. Fountain, R. J. Arculus, R. W. Kay, Eds. (Elsevier, Amsterdam, 1992), pp. 81–143.
15. J. Francheteau, C. Jaupart, Shen Xian Jie, Kang Wen-Hua, Lee De-Lu, Bai Jia-Chi *et al.*, *Nature* **307**, 32 (1984).
16. P. E. Wannamaker *et al.*, *J. Geophys. Res.* **94**, 14127 (1989).
17. Financial support was provided by NSF grant EAR-9418822 and by a grant from the Chinese Ministry of Geology and Mineral Resources. Phoenix Geophysics (Canada) Ltd. provided V5 time series recording capability and laptop computers. We thank I. Billings and B. Narod for serving as field technicians for the LIMS data acquisition and the staff of the Tibetan Ministry of Geology for support. Geological Survey of Canada contribution number 1996194.

2 August 1996; accepted 5 November 1996

The Origin of the Great Bend of the Nile from SIR-C/X-SAR Imagery

Robert J. Stern and Mohamed Gamal Abdelsalam

The course of the Nile in northern Sudan follows a contorted path through Precambrian bedrock. Radar imagery shows that basement structures control the river's course in this region. Northward-flowing segments follow Precambrian fabrics, whereas east-west segments follow faults of much younger age. These faults may reflect recent uplift of the Nubian Swell and deflection of the river to the southwest to form the great bend of the Nile.

The Nile (6825 km long) (*1*) transports water from high-rainfall regions in Ethiopia and equatorial Africa across the Sahara Desert to Egypt. In northern Sudan, the Nile forms a great bend, first flowing north from Khartoum, then southwest for over 300 km before it resumes its northward course (Fig. 1). Bedrock fabrics are an important control on the course of the Nile in this region (*2*, *3*), although relations between crustal movements and the river's course are poorly understood. Here we present remote sensing data on this part of the Nile, acquired with the SIR-C/X-SAR imaging radar system (*4*) during two flights of the NASA space shuttle Endeavor in 1994. These data reveal how bedrock structures of different age control much of the Nile's course. Many of these structures could be mapped on the ground, but such studies have been inhibited by the size and harsh climate of the study area. Other structures are revealed for the first time by the radar images (*5*).

The evolution of the Nile can be traced from the Late Miocene desiccation of the Mediterranean Sea (*6*). Lowering of the hydrologic base level led to the carving of a deep canyon [2.5 km deep beneath Cairo (*1*)] and vigorous stream piracy upstream from Aswan. Reflooding of the Mediterranean basin at the end of the Miocene drowned this canyon, and sedimentary filling of the estuary produced the broad and fertile Nile floodplains north of Aswan [the "Egyptian region" of (*7*)]. The Cataract region of the Nile extends 1850 km south from the first cataract at Aswan to the sixth cataract just north of Khartoum. Although parts of this region are occupied by broad floodplains, the Nile is mostly incising its channel into Precambrian basement (*8*) (Fig. 1).

We focused on the third, fourth, and fifth cataract stretches. The third cataract stretch extends north over basement exposures from about 19°45′N to Lake Nasser, as the river traverses the Nubian Swell (Fig. 1 and Fig. 2A) (*9*). The fourth cataract stretch extends SW from the bend at Abu Hamed, where the Nile flows over basement rocks for about 200 km before Cretaceous sandstones are encountered (Fig. 1). The fifth cataract stretch extends NNW from Atbara for over 200 km to Abu Hamed (Fig. 2B) and is entirely over Precambrian basement rocks.

Cataract-region Precambrian granitic and metamorphic rocks (Fig. 1) (*10–12*) were covered by Cretaceous sandstones (*13*) affected by 47- to 81-million-year-old igneous intrusions and lava flows (*14*). Volcanic fields younger than 15 million years ago (Ma) are scattered across the Bayuda Desert (*15*). Pleistocene and younger alluvial cover occurs discontinuously along the river's course. Cataract-region rocks preserve three sets of planar fabrics. The early structures formed at about 700 Ma (*10*, *12*), have NE-SW to E-W orientations and are exemplified by the Abu Hamed and Dam et Tor fold-and-thrust belts (Fig. 2B). These structures rarely control the course of the Nile, probably because they generally do not dip steeply. They are overprinted by the younger NNW-trending sinistral Abu Hamed and Abu Dis shear zones in the east (Fig. 2B) (*12*) and the N-S trending Akasha and Kosha shear zones to the west (Fig. 2A). These formed about 600 Ma (*16*) and strongly control the Nile along the third and fifth cataract stretches. There is no evidence for NW-SE Mesozoic rift structures that control much of the course of the Nile in the central Sudan (*17*). E-W steep, normal, or strike-slip faults of late Cretaceous or younger age are common along the third cataract stretch. Faults with this orientation are rarely reported from the Sudan (*18*) but are common in southern Egypt (*19*). Because they affect Cretaceous sedimentary rocks, these faults must be Cretaceous and younger in age. An intrusion is truncated by an E-W fault (Fig. 2A), giving an apparent displacement up to the south. A similar intrusion at Jebel Sheikh (Fig. 2A) yields a K-Ar isochron age of 90 ± 2 Ma (*20*).

At the start of the fourth cataract stretch downstream from Abu Hamed, the river follows the northern margin of the Abu Hamed fold-and-thrust belt. Southwest of this, the river follows multiple channels controlled by NNE and E-W fractures (Fig. 3). The E-W portion of the Nile south of Us Island is controlled by a zone of "highly crushed granite," whereas the NNE-SSW portion of the Nile west of Us Island (Fig. 3) follows easily eroded dikes and "splintered granite" (*21*). A recent change in the river's course is demonstrated by a previously unknown paleochannel 25 km long (Fig. 3), lying as much as 10 km north of the Nile. A shuttle photograph of the region SW of that shown in Fig. 3 shows a north-flowing stream course, now crossed by the Nile. These observations indicate that the course of the Nile along the fourth cataract stretch has recently shifted to the south, due to relative uplift of adjacent regions of the Nubian swell. NNE and E-W structural controls cannot be inferred from the course of the paleochannel, and we infer that fracturing accompanied or followed tectonic uplift. The Nile in Egypt has had dramatic changes in flow regime during Quaternary time (*1*, *22*). These are generally ascribed to climatic changes in Ethiopia and equatorial

Center for Lithospheric Studies, University of Texas at Dallas, Box 830688, Richardson TX 75083–0688, USA.